
Title: Prototype composite membranes of partially reduced graphene oxide/$TiO_2$ for photocatalytic ultrafiltration water treatment under visible light[0]

Author: Chrysoula P. Athanasekou Sergio Morales-Torres Vlassis Likodimos George Em. Romanos Luisa M. Pastrana-Martinez Polycarpos Falaras Joaquim L. Faria José L. Figueiredo Adrián M.T. Silva

PII: S0926-3373(14)00229-X
DOI: http://dx.doi.org/doi:10.1016/j.apcatb.2014.04.012
Reference: APCATB 13279

To appear in: *Applied Catalysis B: Environmental*

Received date: 16-1-2014
Revised date: 4-4-2014
Accepted date: 7-4-2014

Please cite this article as: C.P. Athanasekou, S. Morales-Torres, V. Likodimos, G.Em. Romanos, L.M. Pastrana-Martinez, P. Falaras, J.L. Faria, J.L. Figueiredo, A.M.T. Silva, Prototype composite membranes of partially reduced graphene oxide/$TiO_2$ for photocatalytic ultrafiltration water treatment under visible light[0], *Applied Catalysis B, Environmental* (2014), http://dx.doi.org/10.1016/j.apcatb.2014.04.012

Highlights

- We have achieved to develop vis-light active reduced graphene oxide/$TiO_2$ membranes.
- High stability of graphene oxide/$TiO_2$ achieved on substrates of 10 nm pore size.
- Vis-light activity makes a photocatalytic filtration process more energy efficient.

# Prototype composite membranes of partially reduced graphene oxide/$TiO_2$ for photocatalytic ultrafiltration water treatment under visible light[0]

Chrysoula P. Athanasekou[a], Sergio Morales-Torres[b], Vlassis Likodimos[a,c], George Em. Romanos[a**], Luisa M. Pastrana-Martinez[b], Polycarpos Falaras[a], Joaquim L. Faria[b], José L. Figueiredo [b], Adrián M.T. Silva[b*]

[a]Division of Physical Chemistry, Institute of Advanced Materials, Physicochemical Processes, Nanotechnology and Microsystems (IAMPPNM), NCSR Demokritos, 15310 Aghia Paraskevi, Attikis, Athens, Greece

[b]LCM – Laboratory of Catalysis and Materials – Associate Laboratory LSRE/LCM, Faculdade de Engenharia, Universidade do Porto, Rua Dr. Roberto Frias, 4200-465 Porto, Portugal

[c]Department of Solid State Physics, University of Athens, Panepistimioupolis, GR-157 84 Athens, Greece

∗Corresponding author. Tel.: Tel.: +351 220414908

∗∗Corresponding author. Tel.: +30 2106503972 3

E-mail addresses: groman@chem.demokritos.gr (G. Em. Romanos), adrian@fe.up.pt (A.M.T. Silva).



## Abstract

A highly efficient hybrid photocatalytic/ultrafiltration process is demonstrated for water purification using visible light. The process relies on the development of partially reduced graphene oxide/$TiO_2$ composite membranes and their incorporation into an innovative water

purification device that combines membrane filtration with semiconductor photocatalysis. Composites consisting of graphene oxide sheets decorated with $TiO_2$ nanoparticles were deposited and stabilized into the pores of ultrafiltration mono-channel monoliths using the dip-coating technique. Cross-flow and dead-end filtration experiments were sequentially conducted in dark, under UV and visible light. The membrane surface was irradiated for the elimination of two synthetic azo-dyes, methyl orange and methylene blue, from water solutions. The synergetic effects of graphene oxide on pollutant adsorption and photocatalytic degradation capacity of $TiO_2$ were thoroughly studied, while the influence of the pore size of the monolithic substrate on the deposition morphologies was also elucidated. Moreover, the performance of the novel hybrid process was compared with that of standard nanofiltration with respect to pollutant removal efficiency and energy consumption, providing firm evidence for its economic feasibility and efficiency.

***Keywords:*** Ultrafiltration membranes; titanium dioxide; graphene oxide; azo-dye pollutants; photocatalysis; clean water.

## 1. Introduction

Photocatalytic membranes exhibiting the simultaneous action of pollutant rejection and photocatalytic degradation, have received much attention [1-7] due to the simplicity of the overall water treatment process and the beneficial effects arising from the presence of the photocatalyst on the membrane surface and pores (anti-biofouling, cleaner permeate, higher flux) and vice versa (increased pollutant concentration in the vicinity of the photocatalyst, turbulent flow and efficient mixing due to the asymmetric pore structure of the membrane). Moreover, hybrid photocatalytic membrane processes have the potential to eliminate a major drawback of membrane separation technology, which is the generation of toxic condensates. Since the pioneer work of Barni et al, who described the PHOTOPERM® process [8], and

the succeeding synthesis of composite $TiO_2/Al_2O_3$ membranes with hierarchical mesoporous multilayer structure [9-10], there have been persistent efforts towards the development of efficient photocatalytic membranes with concurrent water filtration and photocatalytic degradation properties. Polymer based [11], free-standing [12] or ceramic [13] based photocatalytic membranes have already been successfully prepared and their anti-fouling, high flux, photodegradation and filtration efficiency has already been proved. Despite their relatively high cost compared to the polymeric candidates, ceramic porous filters are the substrates of choice for developing photocatalytic membranes. Ceramic filters exhibit excellent thermal, chemical, and mechanical properties, while retaining their capacity to be reused after calcination. These characteristics ensure the integrity of the substrate during the deposition, stabilisation and activation of the photocatalyst [14, 15] as well as during the water treatment process under UV irradiation and the concomitant attack by the hydroxyl radicals generated on the photocatalyst. The most common way to develop the photocatalytically active membrane layer is by means of sequential dip-coating of the substrate into appropriate sols composed of different precursor materials, that generate ultrathin layers consisting of nanocrystallites with decreasing size, as we move away from the substrate's surface. The purpose of this multi-coating procedure is to mask support's defects [16, 17] that undermine the integrity of the active top layer. As a more versatile technique, CVD of various metal-organic precursors can effectively control the pore size by depositing either active metal-oxide nanocrystalline layers on the pore mouth of the rough substrate or uniform nanoparticles, which can be smaller than those usually formed by the sol-gel routes.

In former studies of our group, CVD derived double sided active photocatalytic ceramic ultrafiltration (UF) membranes were employed for organic dye removal from wastewater [18-21]. The innovative hybrid photocatalytic/UF process involved the filtration of polluted water in the cross-flow or dead-end membrane configuration, with UV irradiation applied on

both photocatalytically active surfaces of the membranes. The overall concept and method of implementation into an efficient water purification device are already protected by a European patent [22]. When compared to the standard nanofiltration (NF) with ceramic membranes, the hybrid photocatalytic/UF process achieved five times higher pollutant removal efficiency while performing with the same water recovery [21]. Most important, due to the low trans-membrane pressure, the energy expense ($kWh/m^3$) of the pump feeding the water stream in the membrane module was almost half the energy usually spent in NF. However, proper evaluation of the economic feasibility of the proposed hybrid photocatalytic/UF water treatment requires taking also into account the energy consumed for powering the UV sources. The concern is clearly depicted in Figure 1, where the energy consumption of a CVD derived photocatalytic ceramic membrane [21] is compared with the standard NF and RO processes. When applying three or more UVA light sources of 8 W each, with the purpose to achieve sufficient irradiation density on the photocatalytically active membrane surface, the total energy consumed for treating the same amount of water exceeds that required in a typical NF process, and in some cases it is equal to that of the most energy demanding RO.

In this context, the exploitation of cost-free solar energy instead of UV light sources is highly appealing. Following the spreading of visible-light-active materials and technologies using solar radiation, like photovoltaics and optical fibers, attempts to extend the photoresponse of $TiO_2$ into the visible region and exploitation of solar light driven applications has become a topic of great interest. Surface modification of $TiO_2$ by anion or metal doping [23-26], or the development of composites with carbon materials like carbon nanotubes (CNTs), fullerenes, graphene, nanodiamonds and other nanocarbons mainly of graphitic type, have led to significant enhancement of their photocatalytic activity under visible light [27-29].

**FIGURE 1**

Especially the topic of CNTs-$TiO_2$ and graphene oxide (GO)-$TiO_2$ composites has lately attracted much attention by our group [30, 31] due to the manifold and charge transfer effects foreseen when the graphitic surface is coupled with the surface of the photocatalyst.

In the present study, partially reduced graphene oxide/$TiO_2$ composite membranes were developed for a photocatalytic/UF water treatment process activated by visible light. To this aim, ceramic membranes were coated with graphene oxide/$TiO_2$ composites (GOT) and tested in the photocatalytic removal of organic dyes from synthetic wastewater, under continuous flow conditions. Nanofiltration and ultrafiltration ceramic monochannel monoliths were used as substrates with the purpose to unveil the effect of the pore size on the stability and pollutant removal efficiency of the developed GOT photocatalytic membranes. In addition, a $TiO_2$ membrane had been developed by using the same dipping sol but without dispersing GO, in order to have a reference material to compare with the GOT membranes and to elucidate the effect of partially reduced graphene oxide (GO) on the photodegradation and adsorption capacity.

## 2. Experimental.

### *2.1 Materials and reagents.*

Ammonium hexafluorotitanate (IV) (>99.99%), boric acid (>99%), sulphuric acid (>95%), MO (99%) and MB (99%) were obtained from Sigma–Aldrich. The substrates applied for the development of the GOT membranes were silica NF single channel monoliths with nominal pore size of 1 nm and molecular weight cut off (MWCOT) of 0.45 kD and γ-Alumina UF single channel monoliths with nominal pore size of 5 and 10 nm and respective MWCOT of 7.5 kD, and 50 kD. The NF or UF separation layer (1.5 microns in thickness) was located on the shell side of the monolith, which had a length of 15 cm, ID and OD of 7 and 10 mm respectively and glazed ends of 1.5 cm length. The rest of the tubular membrane

from the shell to the lumen side consisted of two intermediate γ-alumina layers and a rough macroporous α-alumina support. Details on the pore size and volume of the several layers can be found elsewhere [32].

Natural graphite (99.9995% purity, 20 μm, from Sigma–Aldrich) was used as precursor of GO. First, graphite oxide was prepared through the modified Hummers method [33, 34]. Then, the resulting material was dispersed in a given volume of water and sonicated with an ultrasonic processor (UP400S, 24 kHz) for 1 h. The resulting sonicated dispersion was centrifuged for 20 min at 3000 rpm to obtain a suspension of GO.

Then, the GOT composite was synthesized with these dispersions by the liquid phase deposition (LPD) method at room temperature, as described elsewhere [33]. Briefly, ammonium hexafluorotitanate (IV), $(NH_4)_2TiF_6$ (0.1 mol/L), and boric acid, $H_3BO_3$ (0.3 mol/L), were added to a certain amount of the GO dispersion heated at 60°C for 2 h under vigorous stirring. The material was separated by filtration, washed with water and dried at 100°C under vacuum for 2 h. The carbon loading (4 wt.%) was selected taking into account the highest photocatalytic activity obtained with this GOT composite in our previous work [33]. Bare $TiO_2$ was also prepared and treated by the same method, without the addition of any carbon material.

### *2.2 Membrane development.*

An aqueous dispersion (50 g/L) containing the corresponding photocatalyst (GOT or bare $TiO_2$) was used to deposit the material on the different ceramic membranes by dip-coating (down/up velocity of 50 mm/min and dip time of 30 seconds). Three layers were applied on the membranes and after each coating layer the membrane was dried at 120 ºC in an oven for 30 min. After that, the coated membranes were treated at 200 ºC, with a heating and cooling rate of 1 ºC/min and under a $N_2$ atmosphere. The latter treatment resulted in the enhancement of the composite's photocatalytic activity by the improvement of $TiO_2$ nanoparticle

crystallinity and the partial reduction of the GO sheets that further enhances charge transfer between the composite constituents [33]. Finally, the ceramic membranes were softly flushed with compressed air in order to remove the particles not well-adhered before being used in reaction. The membranes developed on the monoliths with pore size of 1, 5, and 10 nm using the GOT aqueous suspension are referred as GOT-1, GOT-5 and GOT-10, respectively, while the membrane developed on the monolith with pore size of 10 nm using the $TiO_2$ aqueous suspension is referred as reference membrane.

## 2.3 Physicochemical and performance characterization.

### *2.3.1 Physicochemical Characterisation*

Micro-Raman spectroscopy measurements were performed in backscattering configuration on a Renishaw inVia Reflex spectrometer using an $Ar^+$ ion laser ($\lambda$=514.5 nm, 2.41 eV) and a high power near infrared (NIR) diode laser ($\lambda$=785 nm, 1.58 eV) as excitation sources. The laser beam was focused onto the specimens by means of a 50× (NA=0.75) objective, while analysis of the scattered beam was performed on a 250 mm focal length spectrometer along with a 1800 lines/mm diffraction grating and a high-sensitivity CCD detector. Raman mapping on the membrane surfaces was implemented on a motorized feedback-controlled XYZ mapping specimen stage.

The morphology of the GOT composite was determined by scanning electron microscopy (SEM) in a FEI Quanta 400FEG ESEM/EDAX Genesis X4M instrument. The point zero of charge ($pH_{PZC}$) of the powder materials was determined following a pH drift test described elsewhere [35, 36]. Solutions with varying initial pH (2–12) were prepared using HCl (0.1 mol/L) or NaOH (0.1 mol/L) and 50 mL of NaCl (0.01 mol/L) as electrolyte. Each solution was contacted with 0.15 g of the material (GOT or $TiO_2$) and the final pH was measured after 24 hours of continuous stirring at room temperature. The PZC value of the material was

determined by intercepting the obtained final-pH *vs.* initial-pH curve with the straight line final-pH = initial-pH.

### *2.3.2 Performance evaluation*

The hybrid photocatalytic/membrane filtration processes took place in a photocatalytic purification device, which has been described in detail elsewhere [21]. In brief, the purification device allowed to determine the performance of photocatalytic tests in the cross-flow and dead-end filtration mode with irradiation applied on the shell side surface of the single channel monolith. Near-UV radiation (315–380 nm) with a peak at 365 nm, was applied at a light intensity of 2.1 mW $cm^{-2}$. This irradiation density was achieved by four UV lamps of 9 W (Phillips-UVA (PUVA) PL-S/PL-L) placed at a distance of 3 cm from the outer Plexiglas cell of the membrane reactor and sleeved by a cylinder of thick aluminum foil. Four Vis lamps of 9 W (Osram DULUX S 9W/21-840 G23 LUMILUX Cool White), placed at the same distance of 3 cm from the Plexiglas cell, were used to achieve a Vis light irradiation density of 7.2 mW $cm^{-2}$.

The total flow of polluted water feeding the reactor was 1.5 mL/min for the GOT-5, GOT-10 and reference membranes, and the filtration was performed in the dead-end mode. The GOT-1 membrane was examined in the tangential flow (cross-flow) mode with a total polluted water feed of 0.3 mL/min. The concentration of MO and MB in the feed solution was $4.4 \times 10^{-3}$ mg/mL and $1.8 \times 10^{-3}$ mg/mL respectively.

The concentrations ($C$) of MO and MB collected from the retentate and permeate side of the membrane, and the concentration ($C_0$) of the feed, were determined by measuring the visible light absorbance at 466 nm and 664 nm, respectively. The total amounts of removed pollutant were obtained from the mass balance between the feed, retentate and permeate side of the GOT-1 membrane and between the feed and permeate side of the GOT-5, GOT-10 and reference membranes.

## 3. Results and Discussion.

### *3.1 The effect of GO on the adsorption and photocatalytic performance of the membranes.*

Comparative performance evaluation of the GOT modified photocatalytic membrane (GOT-10) and that modified with the respective $TiO_2$ phase (reference) was performed in order to unveil the occurrence or not of synergetic charge transfer and adsorption effects of GO on the photocatalytic activity of $TiO_2$.

The capacity of the two membranes to remove MO and MB from their aqueous solutions was examined in the dead-end filtration mode with a feed flow of 1.5 mL/min. Filtration experiments were sequentially performed, starting without irradiation (in dark) and continuing with UV and Vis irradiation applied on the shell side surface of each membrane. The flow direction of the aqueous solution was from the shell to the lumen side, and the photocatalytically active surface of each membrane was approximately 25 $cm^2$.

Figure 2a presents the retained amount of pollutant (adsorbed and/or rejected) per square centimeter of membrane surface *vs.* the total amount fed in the reactor under dark conditions. The retained amount was calculated from the mass balance between the feed and permeate side of the membrane, and normalized over the active membrane's surface.

**FIGURE 2**

No significant effects due to enhanced adsorption of MB or MO on the GO surface could be identified (Figure 2a). In a previous study of the authors [36], it has been shown that the total pore volume ($V_p$) and BET surface area ($S_{BET}$) are comparable for the GOT composite (0.17 $cm^3/g$ and 110 $m^2/g$, respectively) and $TiO_2$ (0.11 $cm^3/g$ and 120 $m^2/g$, respectively), both being higher than for GO (0.0027 $cm^3/g$ and 21 $m^2/g$, respectively) because aggregation of GO sheets occurs when the suspension of GO is dried to perform $LN_2$ adsorption analysis.

Because of the higher porosity, a beneficial effect on the photocatalytic activity of the GOT-10 membrane could be expected due to increased concentration of the pollutant molecules in the vicinity of the photocatalyst. However, there was no difference on the adsorption performance of GOT-10 compared to the reference membrane (Figure 2a) which might justify a possible significant enhancement of the photodegradation efficiency.

In order to elucidate the reasons behind the similar adsorption capacity of GOT-10 and the reference membranes, the $pH_{PZC}$ of the GOT composite and the possible charge of the pollutant molecules were examined in relation to the pH of the involved solutions. The $pH_{PZC} \approx 3.2$ of GOT treated at 200 ºC reveals a strongly acidic character. Thus, at the pH conditions of the used MO solution (pH = 6.0 at a concentration of 4.4 mg $L^{-1}$) the surface of the composite is negatively charged and the same holds for MO, which has lost its amphoteric character due to deprotonation at the –N=N- bridge between the rings. The same effect occurs in the case of the reference membrane, because $TiO_2$ also presents an acidic character ($pH_{PZC} \approx 3.5$) due to the precursor used in the preparation of this $TiO_2$ material by the LPD method. Concerning the cationic MB dye, both membranes exhibited a 4-fold higher adsorption capacity compared to MO, as expected due to the electrostatic attraction between their negatively charged surfaces (the pH of the MB solution is 7.2) and positively charged ions (Figure 2a). Likewise, the GOT-10 membrane exhibits similar adsorption capacity as the reference, since the employed GOT and $TiO_2$ materials have quite similar $S_{BET}$ and $pH_{PZC}$. On the other hand, the deposition of the GOT composite exerted a negative effect on the flux capacity of the GOT-10 membrane. Figure 2b shows that GOT-10's permeance reached steady state after 4 hours on stream and was considerably lower than that of the reference membrane. The lower permeance of GOT-10 could be attributed to pore-blocking effects induced by the introduction or attachment of the GOT composite into the 10 nm pores of the support. The pore size of 10 nm was sufficient to host the GO-$TiO_2$

composites, ensuring the stability of the derived GOT-10 membrane, in contrast to the supports of smaller pore size (see section 3.2).

Although high flux is a desirable property of membrane technology, it should be noted that the 30-35% reduction in the water permeance of GOT-10 compared to the reference membrane was not so severe and could be effectively compensated by the advantage of high stability.

It is also important to note the continuous decline of the permeance for both membranes during filtration in dark (Figure 2b). This is the result of limitations to the passage of water, posed by the adsorption (stacking) of MO or MB molecules on the active sites of the membrane's surface. The same effect occurs with the reference membrane as evidenced in Figure 3a,b where optical images of the shell side surface of the reference membrane after the MO filtration experiments in dark and under UV, respectively, are compared.

**FIGURE 3**

Moreover, the observed permeance decline cannot be related to the membranes' fouling, which usually results from the adsorption of larger organic molecules such as humic and fulvic acids that block the pore entrances. This effect can be rather related to changes of the membrane's surface chemistry and charge upon adsorption of MO and MB. The permeance levels off when all active sites are occupied, and from this point onwards the flux properties of the membranes reach a steady state (Figure 2b).

Upon completion of the filtration experiment in dark, the UV sources located around the reactor cell were switched on and the experiment under UV irradiation commenced.

Experiments were performed in this sequence in order to enable the distinction between the effect of photocatalytic degradation and the transient adsorption on a fully fresh surface. As concluded from the results presented in Figure 2a, the amount of pollutant adsorbed on the unsaturated membrane surface is high and could have a significant additive effect on the estimated photocatalytic membrane performance. In this context, our primary purpose was to

allow adsorption equilibrium to be reached and then to start the irradiation experiments in order to focus our study solely on the comparison of the photocatalytic efficiency between the two membranes.

The results obtained under UV irradiation are presented in Figure 4a,b. The first significant aspect is the temporal evolution of the membranes permeance under UV (Figure 4b). At the beginning of the irradiation experiment, the permeance increases as a consequence of the photodegradation of the pre-adsorbed pollutant molecules. In the case of GOT-10, the permeance levels off after 2.0-2.5 hours on stream and remains stable for the next 3.0 hours of the filtration experiment under UV. The stability is due to the continuous degradation of the pollutant molecules that are newly adsorbed on the photocatalyst.

**FIGURE 4**

On the other hand, the permeance of the reference membrane levels off much later and more importantly, its steady state value is 10-13% higher than that obtained at the initial stages of the filtration experiment in dark (Figure 2b). This fact reveals enhancement of the hydrophilic character of the deposited $TiO_2$ during irradiation. The beneficial effects of photoinduced hydrophilicity have already been mentioned in previous studies of the authors concerning $TiO_2$ photocatalysts [37] and photocatalytic membranes. Very recently, a thorough investigation was conducted in order to corroborate the effect of UV irradiation on the flux properties of photocatalytic ceramic membranes. This study confirmed that the observed enhancement of the permeance is not due to warming up of the filtration fluid but rather due to the inherent property of $TiO_2$ to increase the population of surface hydroxyls when irradiated with UV [23]. In the case of the GOT-10 membrane such an effect was not evident, indicating that GO prevents the high hydrophilic character of irradiated $TiO_2$.

Furthermore, a sudden drop in the permeance of both membranes was observed at about one hour after switching from UV to Vis light irradiation (Figure 4d). During MB filtration, the permeance of the reference membrane dropped well below the value of 30 $L/m^2/h/bar$ (the

initial permeance value), indicating that the reference $TiO_2$ material exhibits moderate efficiency for the photocatalytic degradation of MB under visible light. As a result, adsorption of MB molecules causes a significant decrease of the water flux. On the contrary, the steady state permeance value of the GOT-10 membrane under visible light, was almost identical to that obtained during the initial stage of filtration in dark (Figure 2b), a fact unveiling continuous degradation of the newly adsorbed pollutant molecules under Vis light irradiation. The plots of MO and MB removal *vs.* the amount fed (Figure 4a,c) reveal the higher photocatalytic activity of GOT-10 compared to the reference membrane. The enhancing effect of GO is significant and by comparing the slopes of the plots, a 2-fold higher pollutant removal efficiency is concluded for GOT-10.

As already shown, the adsorption capacity of the two membranes was similar. Therefore, electron sinking effects are concluded by the fact that GOT-10 is much more efficient than the reference membrane in the degradation of MB under UV.

Moreover, the much higher activity of GOT-10 under Vis light can be attributed to the fact that GO (4 wt.%) acts as sensitizer (electron donor) of $TiO_2$ under Vis light, as already proved in our previous publication where this material, prepared by the LPD method, was tested in the form of powder [33, 38]. In fact, this GOT composite, independently of its mode of application, either freely dispersed in water [33], immobilized into hollow fibres [36] or stabilized into the pores of UF membranes (as shown in the present work), exhibits remarkable photocatalytic activity under Vis-light.

Finally, we should note that when the target is to compare between the photocatalytic efficiency of different membranes, a filtration experiment of prolonged period under dark must precede the filtration under irradiation. Indeed, when examining a freshly prepared sample, unoccupied adsorption sites are available both on the photocatalytic and non-photocatalytic part of the entire membrane. In that case, differences in the adsorption capacity can lead to misleading conclusions relevant to the ranking of the photocatalytic

efficiency, since adsorption on photocatalytically inactive sites and photocatalytic degradation may occur simultaneously. This is clearly depicted in Figure 5, where we present the pollutant removal efficiency of the membranes for the cases when filtration in dark preceded or not the irradiation experiments. It can be seen that when the irradiation was applied from the beginning of the filtration experiment, the reference membrane presented similar (for MB) or slightly better (for MO) performance compared to GOT-10.

**FIGURE 5**

However, as the filtration proceeds and upon occupation of all active sites with adsorbed molecules the slopes of the plots (Figure 5) decline, especially those corresponding to the reference membrane (compare between Figure 5a and Figure 5b) and the steady state performance highlights GOT-10 as the most efficient photocatalyst.

*3.2 Effect of the substrate pore size on the GOT membranes morphology and performance.*

To determine the optimum pore size of the ceramic support for the development of an efficient and stable membrane hosting partially reduced graphene oxide/$TiO_2$ composites, GOT-10, GOT-5 and GOT-1 membranes were comparatively evaluated for the removal of both MO and MB under dark and UV light conditions. Both the UV photocatalytic efficiency and adsorption capacity in dark of GOT-5 differed markedly from those of GOT-10 and the reference membranes (Figure 6a,b), indicative of significant variations in the deposition efficiency of GOT on membranes of different pore sizes by dip coating.

**FIGURE 6**

The photocatalytic efficiency of GOT-5 was markedly reduced for both MO and MB pollutants, implying a drastic reduction of the amount of photocatalyst deposited on the 5 nm substrate. As evidenced by the corresponding micro-Raman analysis (described below), a relatively smaller fraction of the GOT composite is introduced and stabilized into the 5 nm

pores, while a substantial amount of GOT is rejected and leached out of the membrane's surface.

The photocatalytic efficiency of GOT-5 is much lower than that of GOT-10 and reference membranes (Figure 6b), confirming that less GOT was stabilized into the pores and surface of GOT-5 in comparison to the GOT-10 membrane.

On the contrary, GOT-5 exhibited significantly higher adsorption efficiency in dark compared to both the reference and the GOT-10 membranes. This can be explained in terms of the larger fraction of the γ-alumina surface in direct contact with the solution. At the pH conditions involved, γ-alumina, with a $pH_{PZC}$ of about 9.1, is positively charged and can strongly attract the MO molecules. Indeed, as shown in Figure 6a, GOT-5 presented about 1.5 fold higher adsorption efficiency for MB and 3 fold higher adsorption for MO compared to the reference and GOT-10 membranes.

Besides the photocatalytic efficiency and adsorption capacity, the permeance properties of GOT-5 reflected the lower amount of the photocatalyst stabilized into the membrane pores compared to GOT-10.

During filtration in dark and subsequently under UV, the permeance of GOT-5 (Figure 6c,d) was lower than that of the reference and higher than that of GOT-10 indicating that the phase stabilized into the 5 nm pores did not provoke intense pore blocking as was the case for the GOT-10 membrane. Therefore, the stabilized phase was inferred to be less bulky and/or, more likely, the pores of the γ-alumina layer failed to host most of the GOT composite structures in the GOT-5 membrane.

Moreover, the GOT-5 membrane performs the filtration experiment without any significant change in its permeance upon UV irradiation (Figure 6d), in contrast to the other two membranes, where the permeance increases continuously due to the higher amount of $TiO_2$ that photodegrades the pre-adsorbed pollutants.

The degree of surface modification for the GOT membranes was directly investigated by micro-Raman spectroscopy under 514.5 and 785 nm laser excitations (Figure 7a and b).

**FIGURE 7**

The GOT-10 membrane exhibited a stable Raman spectrum over its surface, comprising the relatively broad anatase $TiO_2$ Raman modes at lower frequencies (100-700 $cm^{-1}$) arising from the small $TiO_2$ nanoparticles grown by the LPD method (ca. 4 nm). In addition, the broad graphitic G and the defect activated D bands were observed at higher frequencies (1300 - 1700 $cm^{-1}$), characteristic of the GO flakes [33]. In the case of GOT-10, the relative intensity of the most intense $TiO_2$ mode at ~156 $cm^{-1}$ with respect to that of the GO-derived G or D bands was similar to those obtained for GOT in powder form at both 514.5 and 785 nm excitation wavelengths (Figure 7a and b). This confirmed that the GOT sheets were homogeneously deposited and stabilized in the 10 nm pores of the UF layer of the membrane support, retaining their structural integrity. Likewise, the broad anatase $TiO_2$ modes were detected on the surface of the reference membrane with similar spectral characteristics to those for GOT [33], confirming the homogeneous deposition of small (4-5 nm) anatase nanoparticles in the 10 nm UF membrane layer.

On the other hand, as the pore size of the membrane's filtration layer decreased for GOT-5 and GOT-1, a systematic increase of the $TiO_2$ mode Raman intensity relative to that of the G and/or D bands was observed at both laser excitations, indicating inhomogeneous deposition and loss of the GOT composite's integrity on the membrane surface. This was most prominent in the case of GOT-5, where the presence of dark coloured spatial regions was additionally identified on the membrane surface (Figure 7c and d). In these dark regions, only a weak Raman spectrum from anatase nanoparticles could be traced together with two weak modes at 379 and 418 $cm^{-1}$ due to $\alpha$-$Al_2O_3$. This suggests a low amount of $TiO_2$ deposition making visible the inner $\alpha$-$Al_2O_3$ membrane layers [39]. On the other hand, the G and D bands were suppressed in the dark regions, confirming the absence of GO sheets. A

reduction of the overall photocatalyst loading on the GOT-5 membrane as well as leaching of a substantial fraction of GOT sheets leading to an inhomogeneous coverage of the membrane surface could be thus evidenced. For GOT-1 a spatially constant Raman signal over its surface is obtained, comprising a relatively weaker GO Raman spectrum with relatively enhanced $TiO_2$ modes, most likely arising from $TiO_2$ nanoparticles that are not joint with GO sheets. This indicates a homogeneous though sparse surface deposition of the photocatalyst on the NF filtration layer.

A comparison of the performance between GOT-1 and GOT-10 membranes is presented in Figure 8. When the efficiency is evaluated in terms of the effective reduction of the pollutant concentration at the permeate effluent (Figure 8a), then GOT-1 can be classified as the best amongst all the developed membranes. Indeed, GOT-1 membrane has the capacity to hinder the passage of the dye molecules to the permeate side rejecting them to the retentate effluent.

**FIGURE 8**

On the other hand, when the target is to degrade (e.g. photocatalytically) the pollutant from both effluents (permeate and retentate), then GOT-1 and GOT-10 membranes display similar performance (Figure 8c).

It is important to note that there have been major differences on the implementation of the photocatalytic filtration experiments between GOT-1 and GOT-10 that may create the impression of similar performance. In particular, due to limitations at the maximum operating pressure of the photocatalytic membrane reactor (a Plexiglas cell was involved to make possible the irradiation on the shell surface of the membrane), trans-membrane pressures could not exceed 20 bar. The pressure limitation in combination with the very low permeance of the GOT-1 membrane (NF regime), necessitated its examination in the cross-flow (tangential flow) filtration mode at a very low total flow rate of 0.3 mL/min. Under these conditions the water recovery achieved was 27 and 32% for the MB and MO experiments, respectively. On the contrary, the GOT-10 membrane was tested in the dead-

end filtration mode at a total flow rate of 1.5 mL/min and water recovery of 100%. It can be concluded that in the case of GOT-1, the contact time of the solution with the photocatalytically active surfaces was about 5 times higher than the respective one with GOT-10. Notably, the large difference in the contact time only partially explains why GOT-1, while bearing less amount of photocatalyst, exhibits similar pollutant removal efficiency to GOT-10. The true reason was the failure to fully saturate the active sites of GOT-1 during the filtration experiment in dark, which preceded the experiment under UV. Indeed, as observed in Figure 8d, the MB adsorption curve was still linear when the UV experiment started.

It is also important to examine the evolution of the concentration of pollutants at the retentate effluent during the filtration experiments under UV (Figure 8b). As mentioned above, at the beginning of the UV filtration with the MB solution, the shell side surface of GOT-1 still possessed a high population of active sites, where MB molecules could be easily adsorbed. Thus, contrary to what would be expected due to size exclusion, adsorption on the surface led to a significant attenuation of the MB concentration in the retentate effluent. The reduction of the concentration could not be attributed to the enhanced photodegradation efficiency of the shell side surface of the membrane, which, as concluded from the Raman analysis, bears a relatively lower quantity of the photocatalyst.

In the case of MO, and just before starting the irradiation experiment with UV, the GOT-1 surface had already been saturated with the pollutant molecules (Figure 8d). With the application of UV, the small amount of the stabilized photocatalyst was not sufficient to photodegrade the MO molecules and moreover, due to the size exclusion effect from the 1 nm pores, the retentate effluent became progressively more concentrated than the feed stream.

Another interesting feature (Figure 9d) is the higher MO and MB adsorption capacity of GOT-1 compared to the GOT-10 membrane. The higher adsorption capacity was due to the

silica NF layer of the monolith that was used as substrate for the development of GOT-1. As concluded from the Raman analysis, photocatalyst particles were only sparsely deposited on the external silica surface of GOT-1, allowing for the direct interaction of most of the silica layer with the pollutant molecules. In this context, the GOT-1 membrane mainly consists of the silica NF monolith ($pH_{PZC} \approx 2.5$) and, thus, at the pH of the experiments (6.0-7.2) the membrane is negatively charged, while MB is positively charged (pKa less than 1 and in the cationic form above this value [40] and MO is negatively charged above 4.2 [41]). Even so, for low mass of pollutants loaded into the reactor, Figure 8d shows that the removal of these pollutants (in dark) is quite similar when the GOT-1 membrane is employed. In the case of the GOT-10 membrane, it consists of a γ-alumina UF monolith ($pH_{PZC} \approx 9.1$) [42]. Alumina is positively charged at the operating pH conditions and, thus, the adsorption of MB (positive) is expected to be quite low and that of MO (negative) quite high in a bare alumina membrane. However, the adsorption of MB is significantly higher than that of MO, demonstrating that GOT was really deposited on this membrane; i.e. since the $pH_{PZC}$ of the GOT composite is near 3.2, the GOT-10 membrane is negatively charged at the pH of the experiments (6.0-7.2) and MB is preferentially adsorbed in comparison with MO.

### *3.3 Comparison of the performance in terms of pollutant removal efficiency and energy efficiency of the process.*

Table 1 presents the operation parameters and efficiency of the photocatalytic filtration process for each of the membranes developed in this work. The performance results indicate that GOT-10 was the best amongst the developed membranes.

**TABLE 1**

With the GOT-10 membrane, the hybrid process exhibited a 4-8 fold higher pollutant removal efficiency (4-fold for MO and 8-fold for MB) compared to GOT-1, while simultaneously consuming about 13 times less energy for the pump that delivers polluted

water to the reactor. Having evidenced that the GOT-1 membrane failed to retain significant amounts from the GOT composite, the respective performance results can be regarded as those of a standard NF membrane with 1 nm nominal pore size. In this context, if the efficiency of the membranes is evaluated in accordance to their capacity to reduce the dyes concentration ($C/C_0$) at the permeate effluent, then GOT-1 is 2-4 times more efficient than GOT-10. Despite this difference, it can be estimated that the GOT-10 membrane could achieve identical performance to GOT-1 under Vis-light (performance expressed in terms of pollutant concentration reduction at the permeate) via recycling 5 and 10 times of the MB and MO permeate effluents, respectively. This is translated to 5 and 10 times higher energy consumption, which, nevertheless, is still lower than the energy consumption of GOT-1.

Figure 9a, demonstrates the beneficial effect of irradiation on the energy expense of the photocatalytic ultrafiltration process focusing on the results obtained for GOT-10.

**FIGURE 9**

The ordinate in the plot corresponds to the energy consumed by the pump that delivered the fluid to the reactor while the abscissa is the amount of pollutant removed by GOT-10 up to a certain energy expense. It can be seen that during filtration in dark, the energy consumed increases exponentially, a trend that is consistent with the continuous decline of the membrane's permeance caused by the adsorption of the pollutant molecules on its surface.

On the other hand, the data of the filtration experiments under UV fit well to a logarithmic function, a behavior that can be related to the sudden increase of the permeance at the initial stages of the experiment under UV (photocatalytic degradation of the pre-adsorbed pollutant molecules, Figure 4b). Furthermore, the plots of energy expense *vs.* the amount of pollutant removed under Vis irradiation are almost linear. The underlying reason is that the Vis-light experiment started immediately after the filtration experiment under UV. Thus, due to the Vis-light photocatalytic activity of the GOT-10 membrane, the population of surface

adsorbed molecules remained unchanged and as a consequence there was not significant alteration on the flux capacity of the membrane.

Figure 9b compares the efficiency and energy consumption of GOT-10 and GOT-1 membranes, taking also into account the energy expense of the UV source that irradiated the GOT-10 surface. In particular, the energy consumed by 4 UV sources of 9 W each was added to that consumed by the pump during the entire experimental period. The presented plots are very illustrative of the importance to achieve the development of Vis-light active photocatalytic ceramic membranes and the challenge to design a hybrid photocatalytic/ultrafiltration process, where solar irradiation will be exploited at the maximum possible level.

Although the presented results were obtained in a laboratory scale reactor, where the small size of the involved membrane surface (one monolith of 30 $cm^2$) does not provide the flexibility for appropriate process design and optimization of the irradiation density, it can be concluded that in a hybrid photocatalysis/UF process the most energy consuming component is the light source. Thus, besides the many other benefits offered by photocatalytic/UF (less fouling of the membranes, high flux, no toxic condensates) the economic sustainability and potential industrial application of the process will depend on the efficient development of Vis-light highly active membranes that use solar irradiation.

## 4. Conclusions.

Partially reduced graphene oxide/$TiO_2$ membranes were developed by the deposition of GOT composites on ceramic UF and NF monoliths via dip coating. The pore size of the monolith was crucial for the amount of the GOT composite stabilized on the substrate and for the Vis-light photocatalytic efficiency of the developed GOT membranes. It has been concluded that only the membrane developed on the UF monolith with 10 nm pore size

exhibited enhanced photocatalytic performance under visible light. This was attributed to the capacity of the 10 nm pores to host the GOT composites, whereas a sparse deposition of $TiO_2$, the active photocatalyst, was achieved in the membranes developed on the monoliths with pore sizes of 1 and 5 nm.

The performance of a hybrid photocatalysis/UF process involving the GOT-10 membrane was improved compared to that of a standard NF process in regard to the overall dye removal capacity and to the dye concentration reduction in the permeate effluent.

The liquid phase deposition method involved to develop the GOT composites and their further stabilisation on to ceramic monoliths via dip coating are easily up scalable and the hybrid photocatalysis/UF process can be easily transferred to an industrial scale application for the removal of azo-dyes from water, utilising a multitude of monoliths with higher length. It can be estimated that a photocatalytic membrane reactor module accommodating 30 monoliths of 1 meter length is sufficient to produce 1 $m^3$ of water per day at an energy expense of 4-5 kWh / 100$m^3$ which is about 20 times lower compared to a standard NF process. Prerequisite for this is that solar light is used as the only irradiation source, something that could be achieved with the graphene oxide/$TiO_2$ membranes developed in this work.

**Acknowledgements.**

Financial support for this work was provided by project PTDC/AAC-AMB/122312/2010, co-financed by FCT (Fundação para a Ciência e a Tecnologia) and FEDER through Programme COMPETE (FCOMP-01-0124-FEDER-019503). This work was also co-financed by FCT and FEDER through project PEst-C/EQB/LA0020/2013 (COMPETE), and by QREN, ON2 and FEDER through project NORTE-07-0162-FEDER-000050. SMT and LMPM acknowledge financial support from SFRH/BPD/74239/2010 and SFRH/BPD/88964/2012, respectively. A.M.T. Silva acknowledges the FCT Investigator

2013 Programme (IF/01501/2013), with financing from the European Social Fund and the Human Potential Operational Programme. The authors also acknowledge financial support by the European Commission (Clean Water - Grant Agreement nº 227017).

**References.**

[1] H. Bai, Z. Liu, D. Delai Sun, Chem. Commun. 46 (2010) 6542-6544.

[2] L. Liu, Z. Liu, H. Bai, D. Delai Sun, Water Res. 46 (2012) 1101-1112.

[3] X. Zhang, D. K. Wang, D. R. S. Lopez, J. C. Diniz da Costa, Chem. Eng. J. 236 (2014) 314-322.

[4] V. Tajer-Kajinebaf, H. Sarpoolaky, T. Mohammadi, Ceram. Int. 40 (2014) 1747-1757.

[5] G.Q. Shao, Adv. Mat. Res. 781-784 (2013) 2124-2128.

[6] M. Li, G. Huang , Y. Qiao, J. Wang, , Z. Liu, , X. Liu, Y. Mei, Nanotechnology 24 (2013) Ar. Number 305706

[7] J. Mendret, M. Hatat-Fraile, M. Rivallin, S. Brosillon, Sep. Purif. Technol.111 (2013) 9-19.

[8] B. Barni, A. Cavicchioli, E. Riva, L. Zanoni, F. Bignoli, I. R. Bellobono, F. Gianturco, A. De Giorgi, H. Muntau, L. Montanarella, S. Facchetti, L. Castellano, Chemosphere 30 (1995) 1861-1874.

[9] H. Choi, E. Stathatos, D. D. Dionysiou, Applied Catalysis B: Environmental 63 (2006) 60-67.

[10] H. Choi, A. C. Sofranko, D. D. Dionysiou, Adv. Funct. Mater. 16 (2006) 1067-1074.

[11] S. S. Madaeni, N. Ghaemi, J. Membrane Sci. 303 (2007) 221-233.

[12] S. P. Albu, A. Ghicov, J.M. Macak, R. Hahn, P. Schmuki, Nano Lett. 7 (2007) 1286-1289.

[13] Z. Zhou, W.-G. Wang, W. Huang, W.-H. Jing, W.-H. Xing, Adv. Mat. Res. 79-82 (2009) 791-794.

[14] Y. S. Lin, Sep. Purif. Technol. 25 (2001) 39–55.

[15] L.G.A. van de Water, T. Maschmeyer, Top. Catal. 29 (2004) 67–77.

[16] A. J. Burggraaf, L. Cot, General overview, trends and prospects, in: A. J. Burggraaf, L. Cot (Eds.), Fundamentals of Inorganic Membrane Science and Technology, Elsevier, Amsterdam, The Netherlands, 1996, 1–20.

[17] A. Alem, H. Sarpoolaky, M. Keshmiri, J. Eur. Ceram. Soc. 29 (2009) 629–635.

[18] G. Em. Romanos, C. P. Athanasekou, F. K. Katsaros, N. K. Kanellopoulos, D. D. Dionysiou, V. Likodimos, P. Falaras, J. Haz. Mat. 211-212 (2012) 304–316.

[19] S. K. Papageorgiou, F. K. Katsaros, E. P. Favvas, G. Em. Romanos , C. P. Athanasekou, K. G. Beltsios, O. I. Tzialla, P. Falaras, Water Res. 46 (2012) 1858 -1872.

[20] G. E. Romanos, C. P. Athanasekou, V. Likodimos, P. Aloupogiannis, P. Falaras, Ind. Eng. Chem. Res. 52 (2013) 13938−13947.

[21] C. P. Athanasekou, G. E. Romanos, F. K. Katsaros, K. Kordatos, V. Likodimos, P. Falaras, J. Membrane Sci. 392 (2012) 192– 203.

[22] P. Falaras, G. Romanos, P. Aloupogiannis, Photocatalytic Purification Device, Application number EP10275076.7.

[23] N. G. Moustakas, F. K. Katsaros, A. G. Kontos, G. Em. Romanos, D. D. Dionysiou, P. Falaras, Catal. Today 224 (2014) 56–69.

[24] M. Pelaez, N. T. Nolan, S. C. Pillai, M. K. Seery, P. Falaras, A. G. Kontos, P. S. M. Dunlop, J. W. J. Hamilton, J. A. Byrne, K. O'Shea, M. H. Entezari, D. D. Dionysiou, Appl. Catal. B: Environ. 125 (2012) 331–349.

[25] C. Han, M. Pelaez, V. Likodimos, A. G. Kontos, P. Falaras, K. O'Shea, D. D. Dionysiou, Appl Catal. B: Environ. 107 (2011) 77–87.

[26] N. G. Moustakas, A. G. Kontos, V. Likodimos, F. Katsaros, Appl. Catal. B: Environ. 130 (2013) 14– 24

[27] R. Leary, A. Westwood, Carbon 49 (2011) 741–772.

[28] Y. Zhang, Zi- R. Tang, X. Fu, Yi- J. Xu, ACS Nano 4 (2010) 7303–7314.

[29] L. M. Pastrana-Martínez, S. Morales-Torres, S. A. Carabineiro, J. G. Buijnsters, J. L. Faria, J. L. Figueiredo, A. M. T. Silva, Chem. Plus Chem. 78 (2013) 801-807.

[30] S. Morales-Torres, L. M. Pastrana-Martínez, J. L. Figueiredo, J. L. Faria, A. M. T. Silva, Appl. Surf. Sci. 275 (2013) 361–368.

[31] S. Morales-Torres, L. M. Pastrana-Martínez, J. L. Figueiredo, J. L.Faria, A. M. T. Silva, Environ. Sc. Pollut. Res. 19 (2012) 3676-3687.

[32] O. C. Vangeli, G. E. Romanos, K. G. Beltsios, D. Fokas, C. P. Athanasekou, N. K. Kanellopoulos, J. Membrane Sci. 365 (2010) 366–377.

[33] L. M. Pastrana-Martínez, S. Morales-Torres, V. Likodimos, J. L. Figueiredo, J. L. Faria, P. Falaras, A. M. T. Silva, Appl. Catal. B: Environ. 123 (2012) 241–256.

[34] W. S. Hummers, R.E. Offeman, J. Am. Chem. Soc. 80 (1958) 1339.

[35] G. Newcombe, R. Hayes, M. Drikas, Colloids Surf. A Physicochem. Eng. Asp. 78 (1993) 65–71.

[36] L. M. Pastrana-Martínez, S. Morales-Torres, S. K. Papageorgiou, F. K. Katsaros, G.E. Romanos, J. L. Figueiredo, J. L. Faria, P. Falaras, A. M. T. Silva, Appl. Catal. B: Environ. 142 (2013) 101–111.

[37] A. G. Kontos, M. Pelaez, V. Likodimos, N. Vaenas, D. D. Dionysiou, P. Falaras, Photochem. Photobio. Sc., 10 (2011) 350-354.

[38] L. Pastrana-Martínez, S. Morales-Torres, A. G. Kontos, J. L. Faria, J. M. Doña-Rodríguez, P. Falaras, A. M. T. Silva, Chem. Eng. J. 224 (2013) 17-23.

[39] A. Labropoulos, G. Em. Romanos, E, Kouvelos, P. Falaras, V. Likodimos, M. Francisco, M. C. Kroon, B. Iliev, G. Adamova, Thomas J.S. Schubert, J. Phys. Chem. C 117, (2013)10114–10127.

[40] N. Zaghbani, A. Hafiane, M. Dhahbi, Sep. Purif. Technol. 55 (2007) 117–124.

[41] R. E. de Araujo, A. S. L. Gomes, Cid B. de Araújo, Chem. Phys. Let. 330 (2000) 347-353.

[42] J. Hlavay, K. PolyákJ, J. Col. Inter. Sci. 284 (2005) 71–77.

**Tables**

**Table 1:** Flow and pressure conditions applied during the photocatalytic filtration experiments and performance characteristics of the developed membranes. In all cases the feed flow rate was 1.5 ml/min except from the membrane developed on the support with the pore size of 1 nm (GOT-1) where the flow rate was 0.3 ml/min

| | *Pressure* | *Membrane surface area* | *Removal efficiency* | *$C/C_0$ permeate* | *Energy consumption by the pump* |
|---|---|---|---|---|---|
| | *bar* | *$m^2$* | *$10^4 \times$(mg/min)* | | *kWh/100$m^3$* |
| *Reference MB UV* | *1.34* | *25.1* | *2.2* | *0.86* | *3.7* |
| *Reference MB Vis* | *1.42* | *27.2* | *1.5* | *0.88* | *3.9* |
| *Reference MO UV* | *1.15* | *24.7* | *4.6* | *0.95* | *3.2* |
| *Reference MO Vis* | *1.14* | *26.5* | *1.9* | *0.98* | *3.2* |
| *GOT-10MB dark* | *1.70* | *29.6* | | *N/A* | *4.7* |
| *GOT-10MB UV* | *1.52* | *30.4* | *7.9* | *0.65* | *4.2* |
| *GOT-10MB Vis* | *1.50* | *31.5* | *4.8* | *0.77* | *4.2* |
| *GOT-10MO dark* | *2.30* | *29.3* | | *N/A* | *6.3* |
| *GOT-10MO UV* | *1.55* | *32.8* | *4.9* | *0.92* | *4.3* |
| *GOT-10MO Vis* | *1.83* | *31.5* | *3.5* | *0.94* | *5.1* |
| *GOT-5MB UV* | *1.32* | *20.4* | *2.7* | *0.91* | *3.6* |
| *GOT-5MO UV* | *1.63* | *22.9* | *1.1* | *0.99* | *4.5* |
| *GOT-1 MB UV* | *18.5* | *33.0* | *0.9* | *0.20* | *51* |

| | | | | | |
|---|---|---|---|---|---|
| *GOT-1 MO UV* | *19.1* | *33.0* | *1.4* | *0.48* | *53* |

**Figure Captions**

Figure 1: Bar chart presenting a comparison of the energy consumption between a standard membrane technology and the proposed hybrid photocatalytic/ultrafiltration process. The bars with two colors are for the photocatalytic/ultrafiltration.

Figure 2: (a) Pollutant adsorption and/or rejection efficiency of the GOT-10 and the reference membranes for MB and MO in the dark. (b) The respective evolution of permeance during the filtration experiments in dark.

Figure 3: Photos showing the shell side surface of the reference membrane after the filtration experiments with MO. (a) Filtration experiment in dark. (b) Filtration experiment under UV.

Figure 4: (a) Pollutant removal efficiency of the GOT-10 and reference membranes during filtration under UV. (b) Evolution of the GOT-10 and reference membrane permeance during filtration of the MB and MO solutions with the application of UV. (c) Pollutant removal efficiency of the GOT-10 and reference membranes during filtration under Vis. (d) Evolution of the GOT-10 and reference membrane permeance during filtration of the MO and MB solutions with the application of Vis.

Figure 5: (a) Experiments performed with the UV irradiation applied after having reached pollutant adsorption equilibrium in dark. (b) Experiments performed with the UV irradiation

applied at the beginning of the filtration experiment. (c) MB degradation under Vis light. Circle symbols: Irradiation applied after adsorption equilibrium. Diamond symbols. Irradiation applied at the beginning of the filtration experiment.

Figure 6: Pollutants removal efficiency and permeance evolution of the three membranes developed on UF substrates. (a) Adsorption during filtration with MB and MO in dark. b) MO and MB removal efficiency during filtration under UV. c) Permeance evolution during filtration in dark. d) Permeance evolution during filtration under UV.

Figure 7: Micro-Raman spectra on the surface of the GOT and reference membranes in comparison with the GOT powder at (a) 514.5 and (b) 785 nm laser excitations. Optical images and corresponding Raman spectra on the surface of GOT-5 membrane at (c) 514.5 and (d) 785 nm.

Figure 8: (a) Concentration of the pollutant in the permeate effluent ($C$) normalized by the concentration in the feed stream ($C_0$). (b) Concentration of the pollutant in the retentate effluent ($C$) normalized by the concentration in the feed stream ($C_0$). (c) Pollutants removal efficiency of GOT-1 and GOT-10 during filtration under UV. (d) Pollutants removal efficiency of GOT-1 and GOT-10 during filtration in dark.

Figure 9: (a) Effect of irradiation on the energy expense and efficiency of the GOT-10 membrane. (b) Comparison between the performance of the GOT-10 and GOT-1 membranes.

**Figures**

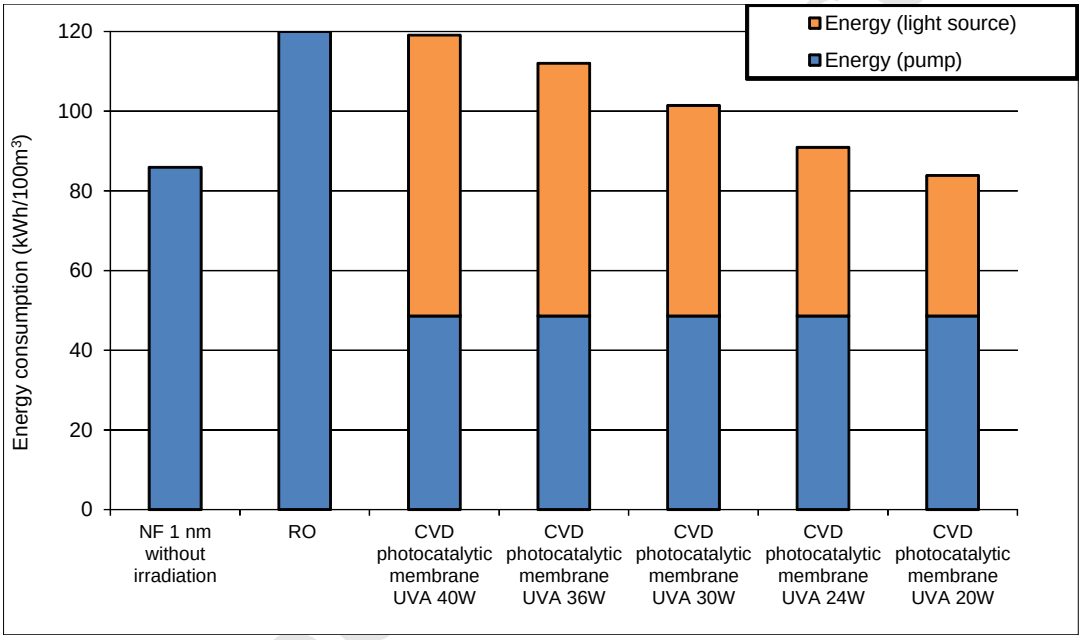


**Fig. 1**

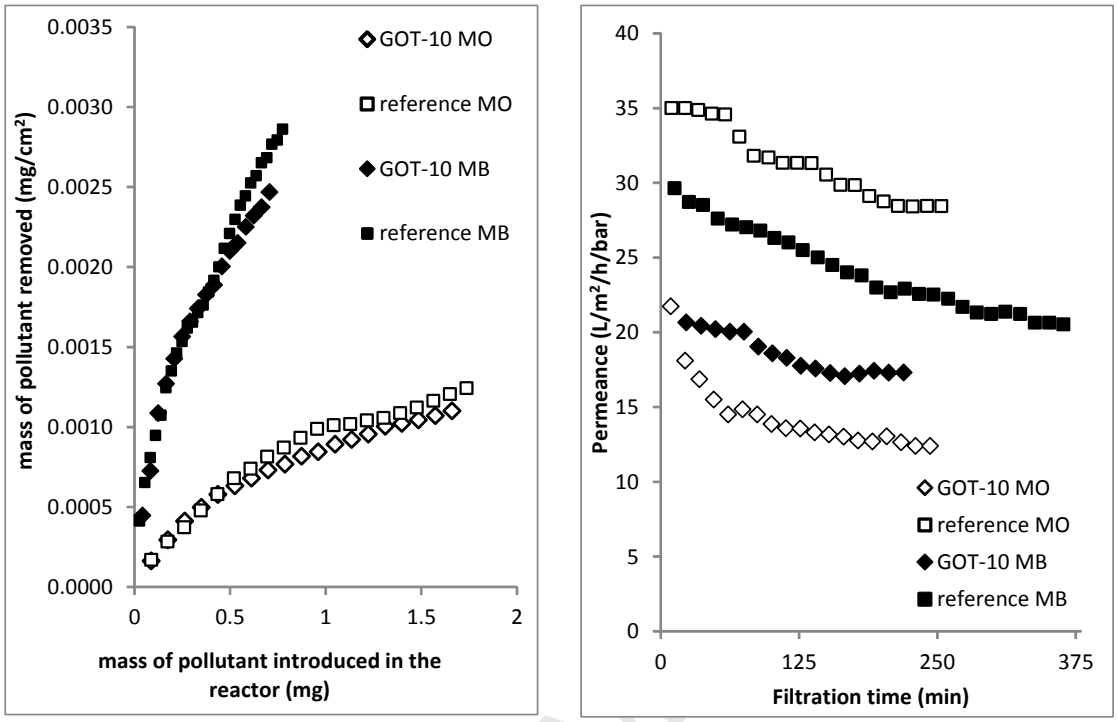


(a) (b)

**Fig. 2**

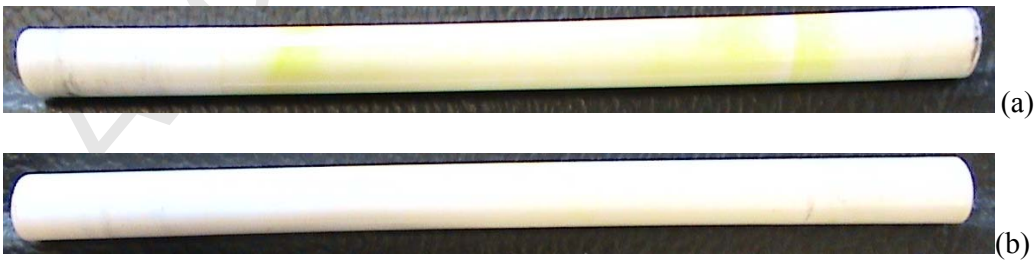

(a)

(b)

**Fig. 3**

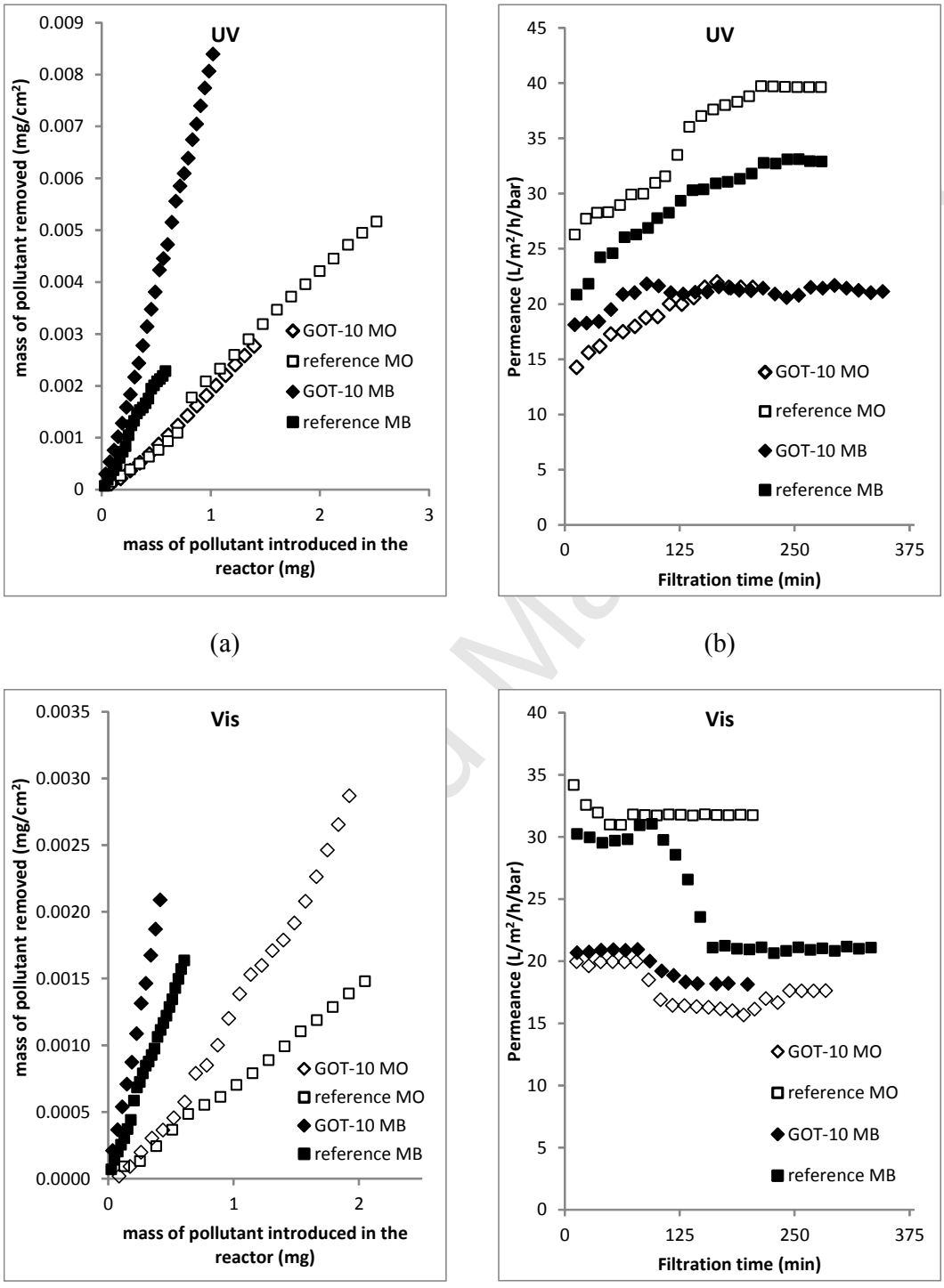


**Fig. 4**

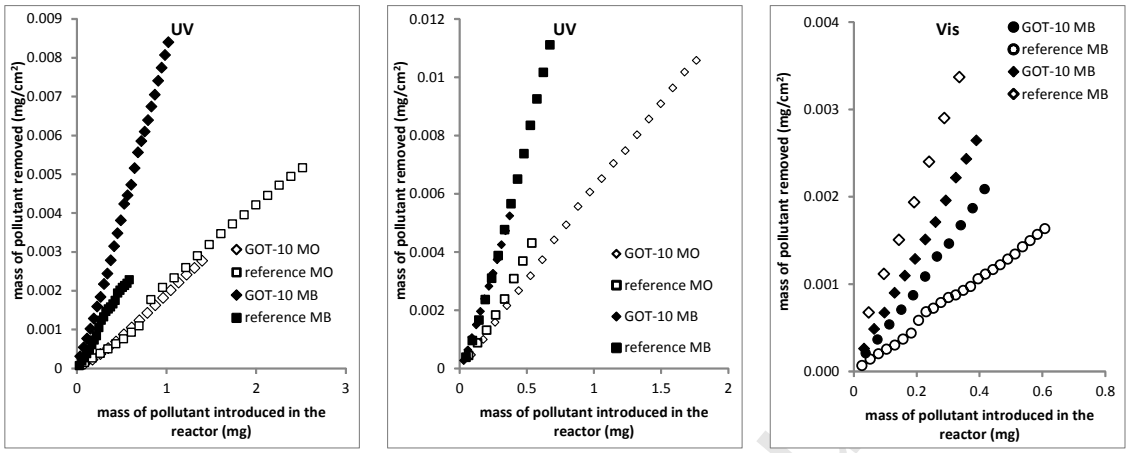


(a) (b) (c)

**Fig. 5**

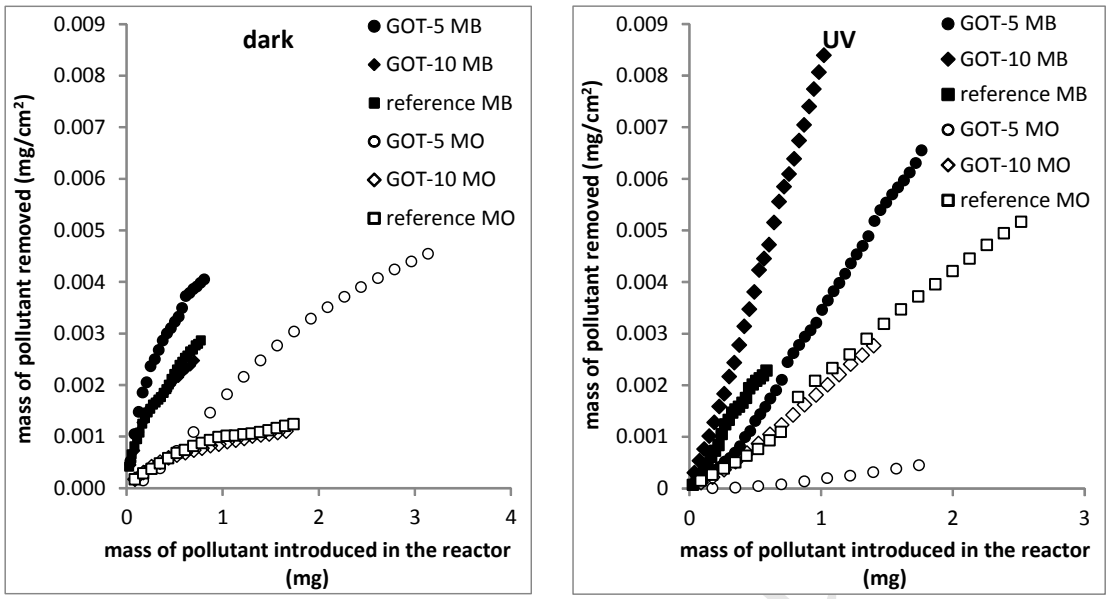


(a) (b)

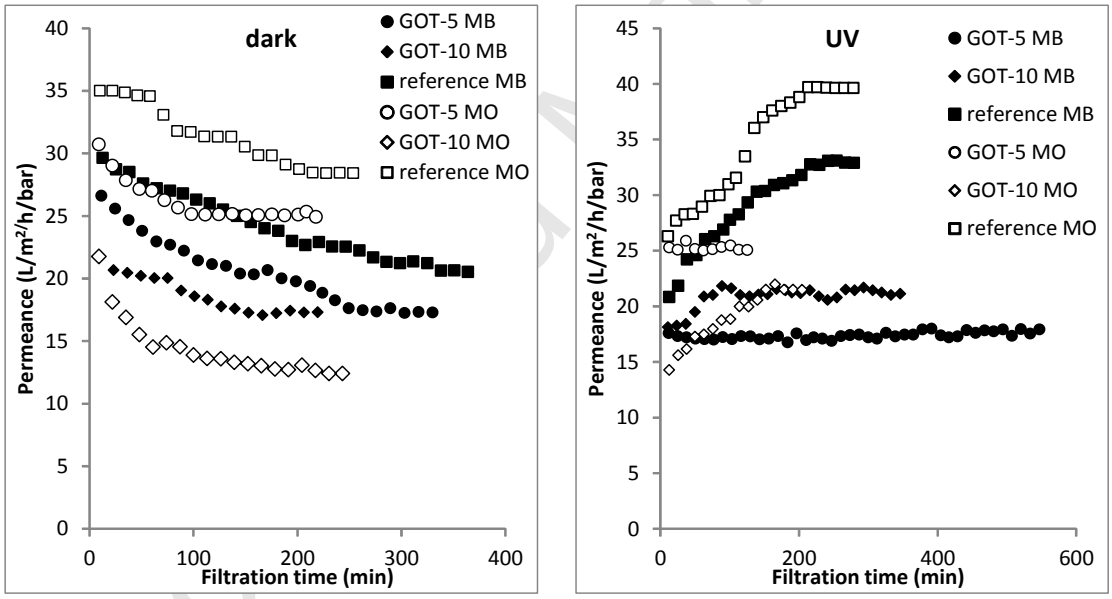


(c) (d)

**Fig. 6**

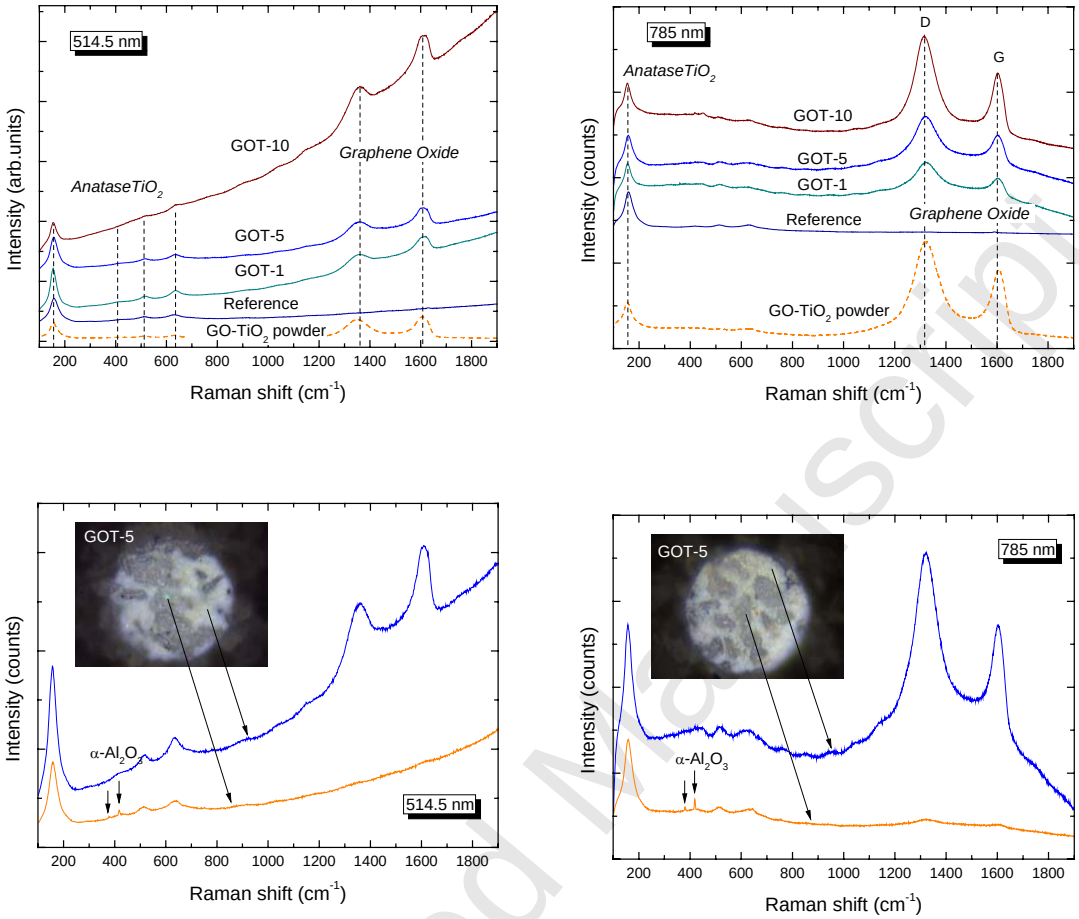


**Fig. 7**

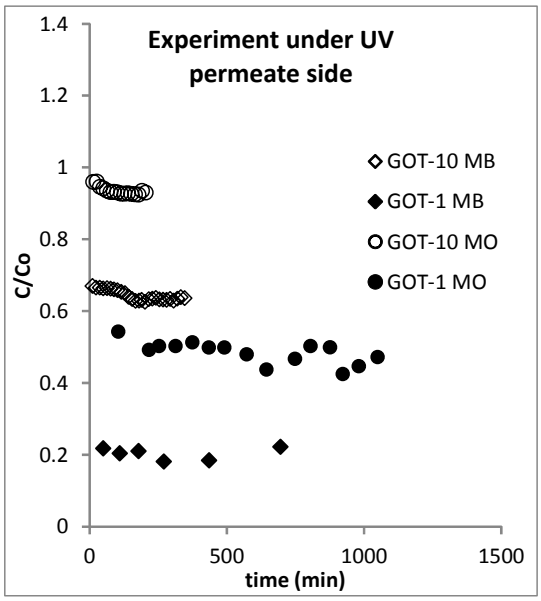


(a)

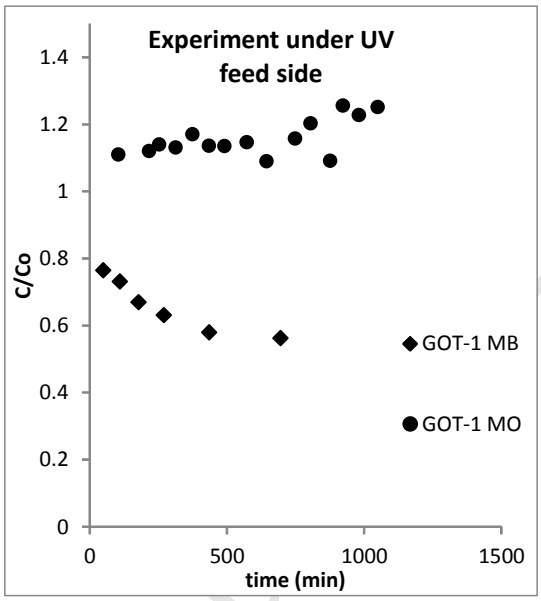


(b)

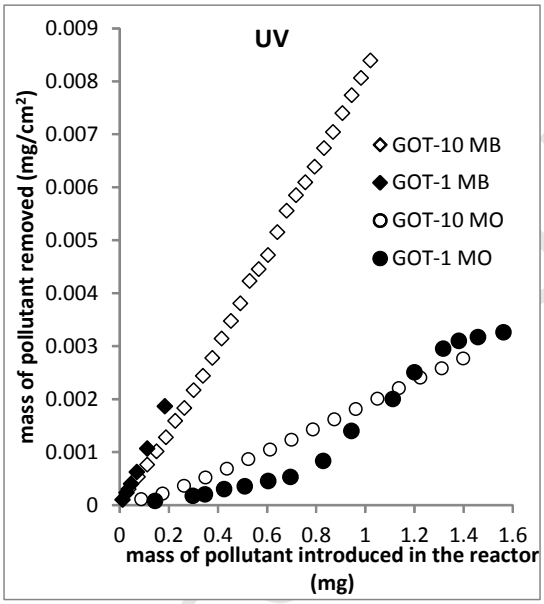


(c)

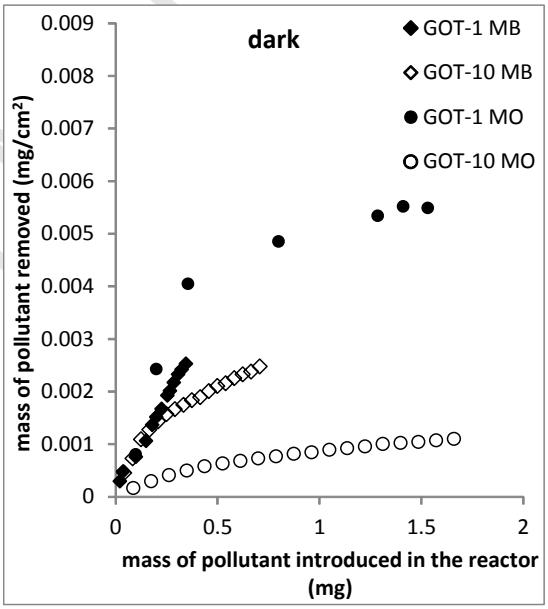


(d)

**Fig. 8**

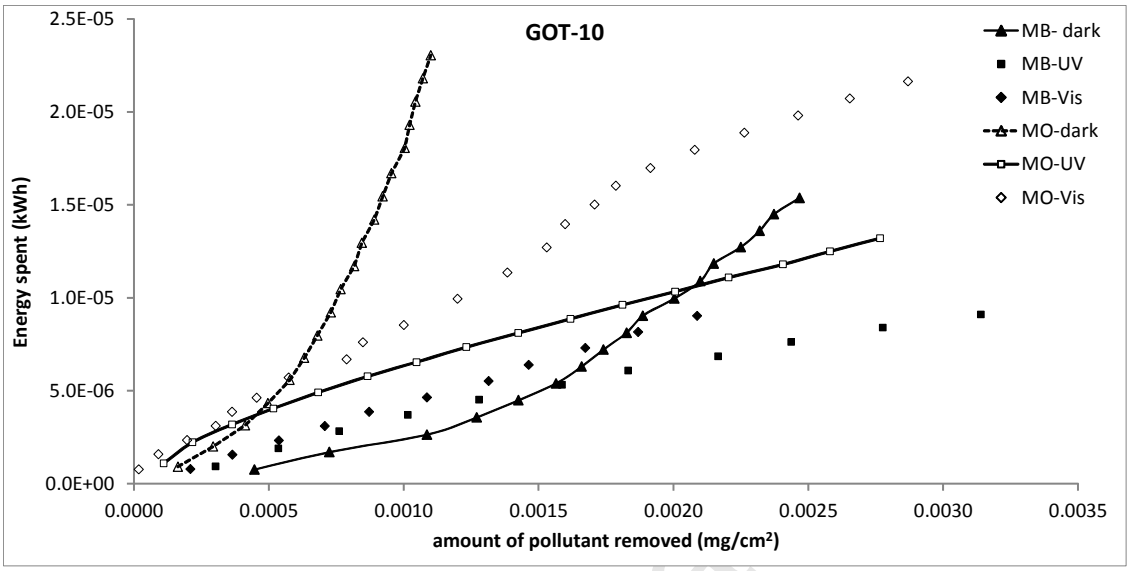


(a)

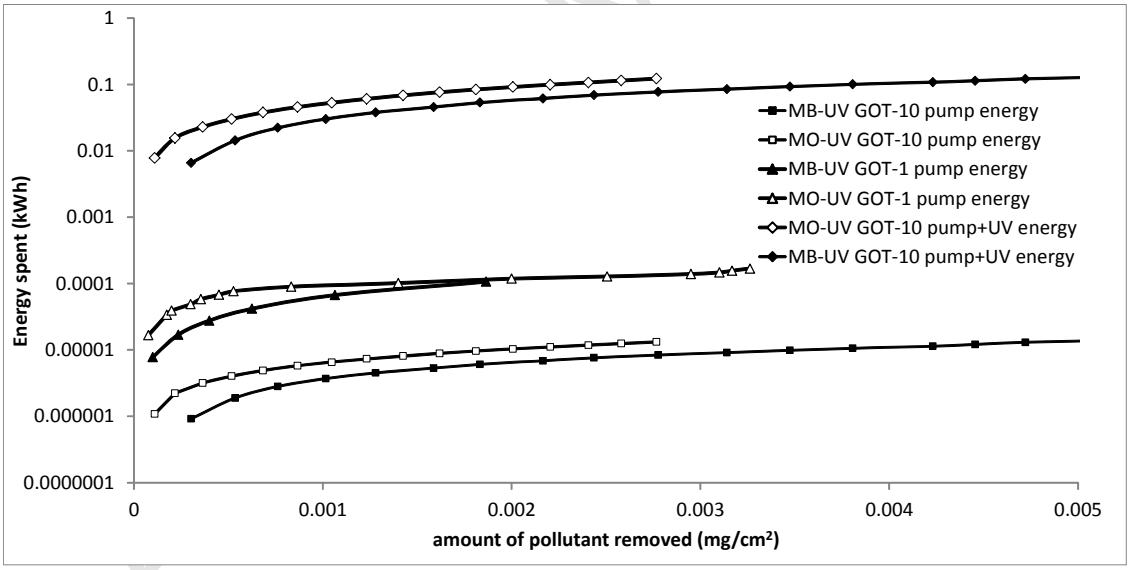


(b)

**Fig. 9**

*Graphical Abstract (for review)

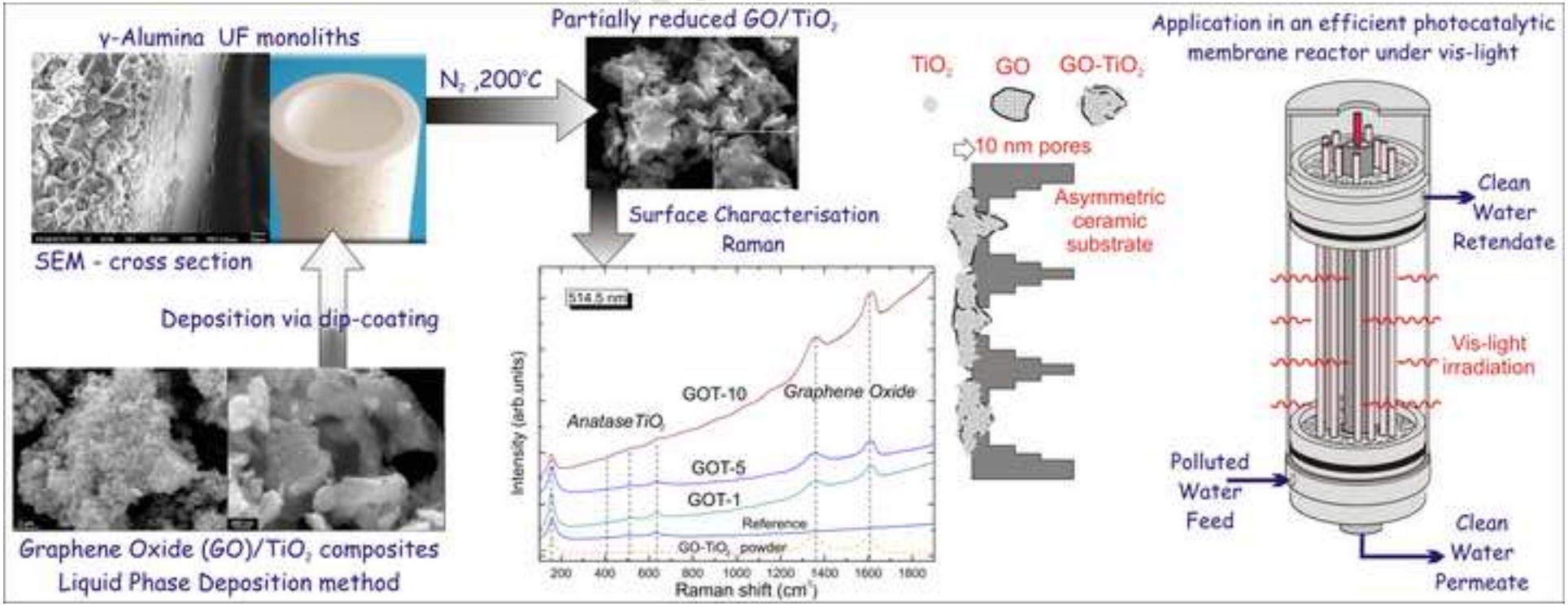

*Graphical Abstract (for review)